Thickness effects on pattern formation in liquid crystals in a rotating magnetic field

Chun Zheng and Robert B. Meyer
The Martin Fisher School of Physics, Brandeis University, Waltham, Massachusetts 02254-9110
(Received 14 August 1996)

We study the thickness effect on solitons and pattern formation in liquid crystals in a rotating magnetic field. When the thickness of a sample is comparable to the coherence length of the magnetic field, it is regarded as ''thin.'' For thin samples, we have found patterns that originate from the flow coupling of dynamic solitons in the synchronous regime. The soliton behavior and pattern formation in thin samples are different from those in the thick ones. For all sample thicknesses in the asynchronous regime, the pattern formation in a nematic cell in a rotating magnetic field can be explained with such important components as instability caused by flow (transient stripes), viscosity reduction mechanism, and phase delay (short-wavelength lattice). The effect of thickness in the synchronous regime can be explained by a scaling method. In the asynchronous regime, the finite thickness affects the pattern responses through its confinement of flow. [S1063-651X(97)06302-2]

PACS number(s): 61.30.Gd, 47.54.+r, 64.70.Md

I. INTRODUCTION

The study of solitons and pattern formation in a nematic cell in a rotating magnetic field has aroused great interest [1–4]. The rotating magnetic field system reveals a rich variety of pattern forming processes and provokes some intriguing questions about the dynamics of nematic liquid crystals driven away from their equilibrium state. We present here our investigations of the thickness effect upon pattern formation in a nematic cell in a rotating magnetic field. Nonintuitive phenomena due to the finite cell thickness have been found. We analyze the pattern formation processes in this system, and provide a complete and consistent picture of solitons and pattern formation in a nematic liquid crystal in a rotating magnetic field.

Our experimental setup is the same as described in [1]. A homeotropically aligned nematic liquid crystal is placed in a horizontal plane and an applied magnetic field rotates in this plane. As the field strength H and angular frequency ω of the applied magnetic field are changed, the sample exhibits different pattern responses. The liquid crystal material we used is El31v, a room temperature liquid crystal mixture manufactured by the British Drug House (BDH) company.

The uniform response of a nematic cell in a rotating magnetic field was studied by Brochard, Leger, and Meyer [5]. There are three different regimes in the response: no distortion (where H is below the Fréedericksz transition), synchronous, and asynchronous (Fig. 1).

When a large enough magnetic field is applied, at the midplane of the sample cell the director will tilt toward the sample plane. Once the magnetic field starts rotating, the director will follow the rotation with a phase lag because of the viscosity. The transition from the undistorted state to the distorted state, which is also known as the Freedericksz transition in a rotating magnetic field, is given by

$$H_c^2(\omega)=\begin{cases} H_c^2\left(1+\dfrac{\omega^2}{\omega_1^2}\right) & (\omega<\omega_1) \quad (1)\\ 2H_c^2 & (\omega>\omega_1), \quad (2)\end{cases}$$

where ω_1 is a parameter constant given by

$$\omega_1=\frac{K_3\pi^2}{\gamma_1 d^2}. \quad (3)$$

Here K_3 is the bend elastic constant, d the thickness of the sample, and γ_1 the rotational viscosity coefficient.

H_c is the critical field for the normal Fréedericksz transition when the field is static. It is determined by the elastic constant (K_3), the thickness d, and the anisotropy of the magnetic susceptibility χ_a:

$$H_c=H_c(0)=\frac{\pi}{d}\sqrt{\frac{K_3}{\chi_a}}. \quad (4)$$

In the synchronous regime, the phase lag between the magnetic field and the local director is a constant which satisfies

$$\sin 2\alpha=\omega\tau, \quad (5)$$

where α is the phase lag and τ is the magnetic field response time given by

$$\tau=\frac{2\gamma_1}{\chi_a H^2}. \quad (6)$$

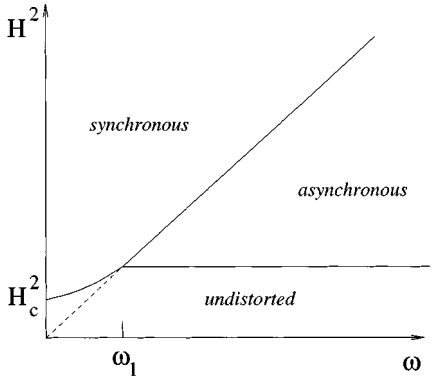

FIG. 1. Schematic state diagram of pattern formation in nematic liquid crystals in a rotating magnetic field. Both H_c^2 and ω_1 scale inversely proportional to d^2.

The transition between the synchronous and asynchronous regimes is prescribed by Eq. (5). When the right hand side of Eq. (5) is larger than 1, α cannot be constant and it goes thus into the asynchronous regime. The condition $\omega\tau=1$ leads to

$$H^2=\frac{2\gamma_1}{\chi_a}\omega. \tag{7}$$

In the asynchronous regime, the local director does not follow the rotation of the magnetic field all the time. A phase slippage occurs (α grows) periodically. The period T of this phase slippage is defined as the time for α to increase by π. The value of T is given by

$$T=\frac{\pi\tau}{\sqrt{\omega^2\tau^2-1}}. \tag{8}$$

The thickness d appears in the expressions of H_c and ω_1. It affects the state diagram in a simple manner: both H_c^2 and ω_1 scale inversely proportional to d^2. Varying the sample thickness will move H_c^2 and ω_1 up or down on the state diagram and enable us to study the pattern responses in different regions in the state diagram (Fig. 2) using convenient values of H and ω.

The above discussion is under the assumption that flow coupling is absent. When flow coupling is considered, the thickness effect is more complex. Inhomogeneous rotation of the director field generates fluid flow, and conversely, a gradient in fluid velocity creates torque on the director. This leads to a positive feedback of flow on director rotation which is responsible for periodic instabilities [6,12] and viscosity reduction [7]. These effects are largest at high rotation rates and low magnetic field, i.e., in the asynchronous regime. Since the flow coupling is important in the asynchronous regime, pattern formation processes in the asynchronous regime are strongly affected by the thickness of the sample. The finite sample thickness serves as a confinement for the flow field. The thinner the sample, the weaker the flow. Both the viscosity reduction lattice with transverse instability (VRL TI) and the Complex pattern are suppressed in thin samples. The reason VRL, which also involves flow coupling, is seen in thin samples is that VRL is a nucleated pattern. Nucleated patterns are generally more stable than spontaneous patterns, such as VRL TI and the complex pattern.

In light of the above discussion, the relative thickness of a sample can be judged on two bases: the magnetic coherence length and the viscous coherence length. The magnetic coherence length is defined as usual by

$$\xi_h=\frac{1}{H}\sqrt{\frac{K_3}{\chi_a}}. \tag{9}$$

It reflects the relative strength of the magnetic field interaction to the elastic force of the medium. The viscous coherence length, on the other hand, is introduced by use of the rotational velocity of the magnetic field ω, and its explicit form is

$$\xi_{\rm vis}=\pi\sqrt{\frac{K_3}{\gamma_1\omega}}. \tag{10}$$

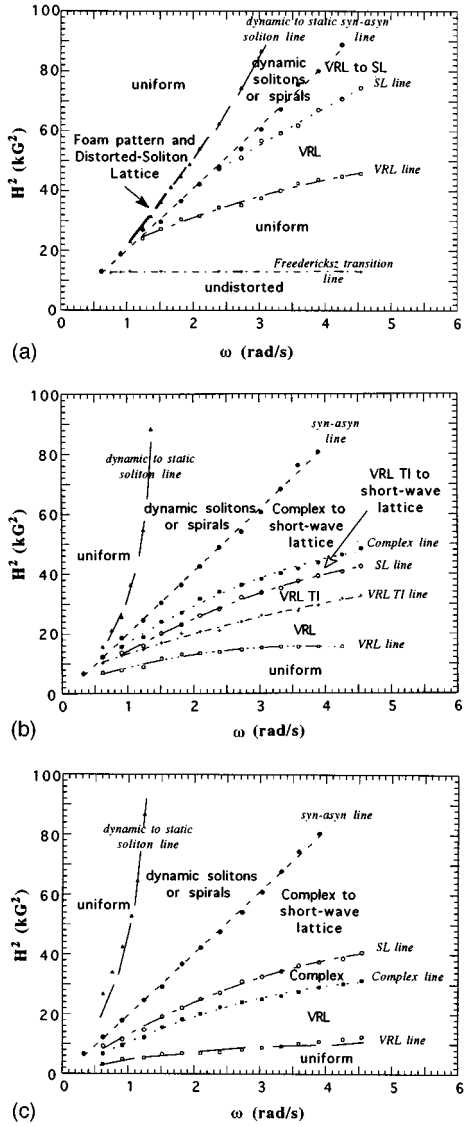

FIG. 2. State diagrams of pattern formation in a nematic cell in a rotating magnetic field. (a) $d=30$ μm, (b) $d=100$ μm, (c) $d=250$ μm. The state diagrams are presented for the short and long time stages; for example, VRL to SL means in the short time period it is the viscosity reduction lattice, while in the long time the VRL is taken over by the short-wavelength lattice. If only one pattern is specified, this pattern persists in both time stages. The Fréedericksz transition line is too low to be seen in (b) and (c). The dynamic to static soliton line in (a) should be viewed as a continuous line; the gradual increase of its thickness indicates that the foam pattern and the distorted soliton lattice form more easily at the lower values of H and ω.

It reflects the relative strength of the viscous force to the elastic force in a rotating magnetic field. These two length scales determine the relative thickness of a sample in the synchronous and asynchronous regimes, respectively. For a thin sample, the ratio of the actual thickness to the appropriate coherence length is small (generally in the range of 3–5).

II. SYNCHRONOUS REGIME

The synchronous regime is characterized by a constant phase lag α between the magnetic field and the local direc-

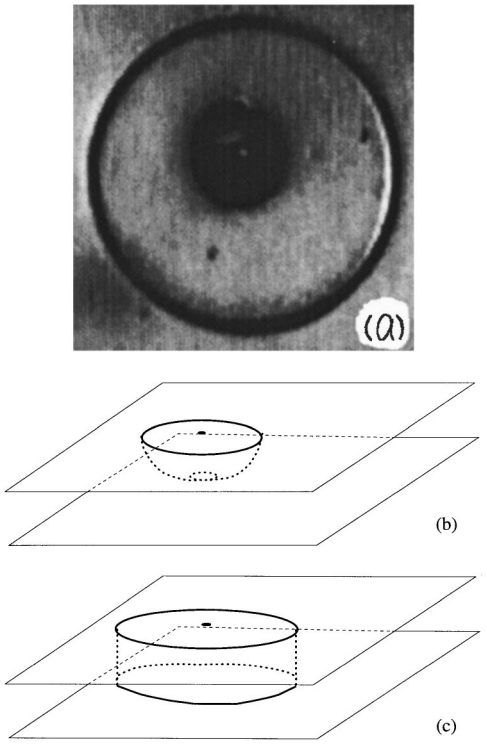

FIG. 3. (a) A three-dimensional soliton. This is a soliton propagating outward from a nucleation point on the top surface. The dark shadow at the center is caused by the soliton touching the bottom surface. After the soliton touches the bottom surface, (b) it moves out quickly across that surface and the soliton converges to a vertical wall (c). $d=250$ μm. Size of image is about 400 μm.

tor. For all sample thicknesses, the synchronous regime can be further divided into two subregimes: dynamic soliton regime and uniform regime. Although a static soliton can be seen in the uniform regime, it is unstable due to the curvature of the ring shape of a soliton. While Migler and Meyer have reported that the transition from a dynamic soliton to a static one is discontinuous and a hysteresis loop exists for this transition, another experiment with a different material has yielded a continuous transition [2]. This phenomenon has been studied [8] separately and the first or second order nature of the transition is found to be controlled by the ratio of the twist elastic constant to the bend and splay elastic constants.

The initial response of a sample in the synchronous regime is uniform. A soliton has to be introduced in one of the following ways: (1) a dust particle in the sample can nucleate a soliton; (2) the lateral boundary is also a nucleating agent; (3) starting from the asynchronous regime with a nonuniform state, we can enter the synchronous regime quickly and introduce solitons; for a thin or clean sample, this is the best way of generating solitons.

Previous studies of solitons in this system have described a soliton as a linelike object separating two areas of the sample. In thick samples, it is more accurate to describe it as a surface separating two volumes of sample. When the sample thickness is large, a soliton can be generated by a dust particle on one surface; it then propagates out from that point as an ellipsoidal front. Figure 3 is a picture of such a soliton which is visible only where it touches the surfaces.

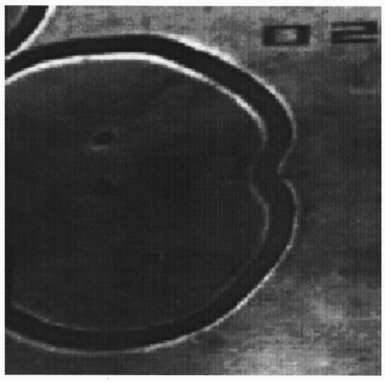

FIG. 4. A snapshot of a distorted soliton in a thin sample. $d=30$ μm. $H=5.7$ kG, $\omega\simeq 1.4$ s^{-1}.

The distortion of the director field in the vertical z direction is basically in twist geometry, while in the xy plane it is bend and splay. Suppose a soliton nucleated on one surface has traveled a distance L horizontally when it touches the other surface. Because the velocity of a soliton is scaled to [9]

$$v_0=\frac{H}{\gamma_1}\sqrt{\chi_a K}, \tag{11}$$

we can infer the ratio of the elastic constants;

$$\frac{\frac{1}{2}(K_1+K_3)}{K_2}\simeq\left(\frac{L}{d}\right)^2. \tag{12}$$

Our estimate from the measurements was $(K_1+K_3)/2K_2 \simeq 1.4\sim 1.6$.

Dynamic solitons and their variation, spirals [10], have been observed for all sample thicknesses (20–250 μm). For very thin samples (20–30 μm) we have also discovered strange behaviors of dynamic solitons along the dynamic-static transition line. There are two independent phenomena to be noted here: a structural instability and the soliton-antisoliton pair.

A normal dynamic soliton has a well defined ring shape due to constant velocity propagation from a nucleation point. In a very thin sample, an instability occurs to the dynamic soliton and the shape of the soliton can be distorted (Fig. 4). This distortion is caused by external fluctuations, such as a local gradient in thickness or a dust particle, but the instability is closely related to the intrinsic structure of the soliton itself [11].

Due to the topology of solitons in a nematic liquid crystal, a soliton is intrinsically an antisoliton relative to the soliton moving in the opposite direction. When a soliton collides with an antisoliton, they annihilate each other since they are topologically attractive [9]. This is not always true in a thin sample. In the same region where we observed the instability of a dynamic soliton, we have also found that a soliton may not annihilate an antisoliton when they collide. Instead, they form a soliton-antisoliton pair which is rather stable. This is a rather strange and nonintuitive phenomenon. We plan to present a study of the soliton pair structure separately [11]. A static foam pattern can be formed by soliton-antisoliton pairs (Fig. 5). If the soliton-antisoliton pairs are distorted by the

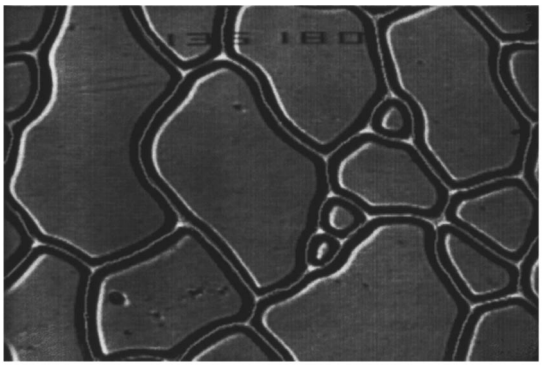

FIG. 5. A snapshot of a foam pattern formed by soliton-antisoliton pairs. $d=30$ μm, $H=5.7$ kG and $\omega\simeq 1.45$ s^{-1}.

structural instability, they grow to fill the entire sample area, forming a static distorted soliton lattice (Fig. 6). Although the structures in Figs. 5 and 6 are static, they are not composed of so-called static solitons. This distinction is that static solitons tend to shrink in length until they disappear, while these do not.

From Fig. 2 it can be seen that both the instability of the soliton and the soliton pair structure are only observed in a narrow window at the lower end of the state diagram along the dynamic to static soliton transition line. When either the magnetic field H or the rotation speed of the field ω is increased, the window gets even narrower and eventually disappears. For large sample thicknesses, this window will be too low in H and ω for the phenomena to be observed easily. Thus the thickness effect in the synchronous regime can be explained by the simple scaling effect of H_c^2 and ω_1.

III. ASYNCHRONOUS REGIME

Contrary to the synchronous regime, the asynchronous regime is described by a periodically growing phase lag α. The pattern formation in the asynchronous regime is better presented in three different time stages, the transient stage, the short-term stage, and the long-term stage.

The transient stage is characterized by a transient stripe pattern (Fig. 7, not shown in the state diagrams Fig. 2). This transient pattern is a spontaneous dynamic response, involving coupled director rotation and fluid flow. It appears and disappears periodically during the phase slippage of the director and the orientation of the stripes also rotates periodically.

FIG. 6. A snapshot of a distorted soliton lattice. Parameters are the same as in Fig. 5.

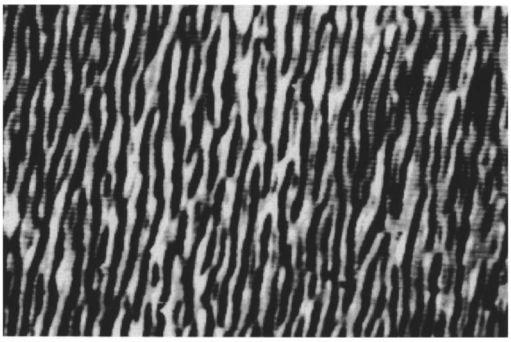

FIG. 7. The transient stripe pattern. This is a snapshot at its maximum amplitude. The pattern is appearing and disappearing periodically and the orientation of the stripes also rotates. Sample thickness $d=100$ μm.

This kind of pattern response has been found in a variety of dynamic systems (see, for example, [6,12]). The basic idea behind the phenomenon is that the periodic response caused by flow coupling of the director has a faster response speed than homogeneous director rotation. The observed stripe pattern is dominated by the fastest growing mode. We have measured the temporal period of this pattern response in our system, which is predicted by Eq. (8) as one would expect (Fig. 8).

Since the transient stripe pattern is caused by flow coupling, the influence of the sample thickness is obvious. As the sample thickness is reduced, flow is suppressed and the stripe pattern is weakened. For a sample of 20 μm, the stripe pattern is not observed.

The short-term stage ranges from a few seconds to about 20 min. Most of the previously studied patterns [1] belong to this stage, including the viscosity reduction lattice, the VRL transverse instability and the complex pattern.

The viscosity reduction lattice (VRL, Fig. 9), as its name suggests, is created by a viscosity reduction mechanism. Although it sounds similar to that of the transient stripe pattern, it is different. The transient stripe pattern is a global spontaneous response, while the VRL is a nucleated one through local interaction. The creation of a VRL needs a certain

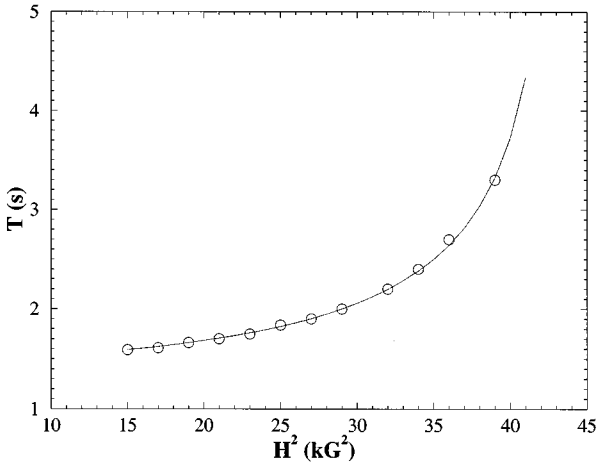

FIG. 8. Measured period of the transient stripe pattern. The circles are measured data; the curve is from Eq. (8). Sample thickness $d=100$ μm, $\omega=2.1$ s^{-1}.

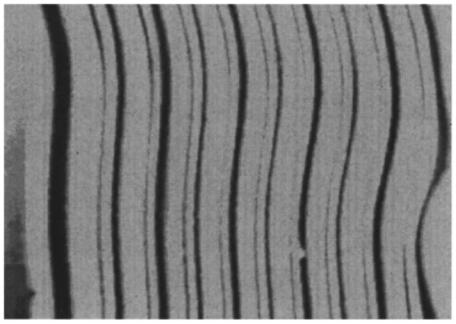

FIG. 9. The viscosity reduction lattice. It is nucleated from the boundary on the right side. Sample thickness $d=100$ μm.

boundary interaction. The boundary causes a gradient in the director field; the gradient of director causes backflow, and the flow acts as a positive feedback to force the local director to move faster. This effectively reduces the rotational viscosity in the vicinity of the boundary. Once the VRL is nucleated, the lattice acts like a boundary itself. New lattice stripes are nucleated at the interface between the lattice and the homogeneous region. Gradually, the VRL grows into the homogeneous region. The mechanism of VRL formation has been studied by Migler and Meyer [7].

The VRL TI is a VRL with transverse instability. It is observed at a higher magnetic field than the VRL. It can be easily identified because of the ripples in the lattice (see Fig. 10, left side). The complex pattern is characterized by a chaotic fluctuation of the director field (Fig. 12).

The fundamental phenomenon in the short-term stage is the VRL. Both VRL TI and the complex pattern are actually the results of interaction between the VRL and the transient stripe pattern. As we increase the magnetic field, while the period of the stripe pattern increases, so does its amplitude (by amplitude we mean the maximum distortion of the local director from its uniform response, and equivalently, the amplitude of flow). This is evidenced by the fact that consecutive stripe patterns may overlap if the amplitude is strong enough, since a higher amplitude takes a longer time to relax. This overlapping of stripes eventually changes the appearance of the stripe pattern, making it a rhombic grid. Starting from a uniform sample, the time for this change to

FIG. 10. The VRL transverse instability. The transverse instability shown in this photo is rather weak, and has a clear direction of orientation. The left part of VRL which is perpendicular to this direction is affected most. The shape of the VRL is determined by the boundary. A more typical VRL TI can be found in [1,9]. Sample thickness $d=40$ μm.

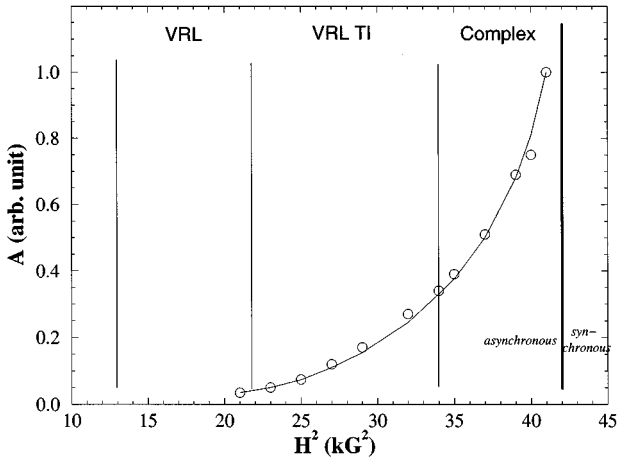

FIG. 11. An indirect measurement of the amplitude of flow corresponding to the transient stripe pattern. The curve is an exponential fit. $d=100$ μm, $\omega=2.1$ s^{-1}.

happen is roughly inversely proportional to the amplitude of the stripe pattern itself. We define the amplitude of the distortion

$$A=\frac{1}{N} \tag{13}$$

where N is the number of cycles of the transient stripe pattern before it changes to a rhombic grid.

From Fig. 11 we can see the influence of the stripe pattern upon the pattern responses in the short-term stage. The VRL region corresponds to minimum amplitude in transient stripe pattern. When the VRL is slightly disturbed by the transient stripe pattern, we have the pattern VRL TI, which is basically the superposition of VRL and the stripe pattern. When the amplitude of the stripe pattern is too large, it destroys VRL and leads to the chaotic complex pattern. Both transitions from VRL to VRL TI and from VRL TI to complex are continuous processes.

The VRL TI shown in Fig. 10 is rather weak in its transverse instability. This is due to the weak flow coupling in a thin sample. It can be seen that the transverse instability has a direction of orientation which corresponds to the direction of the transient stripe pattern. The part of the VRL that is perpendicular to the direction of the transient stripes is af-

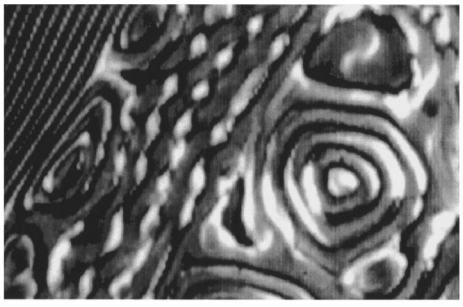

FIG. 12. The short-wavelength lattice is seen at the top left corner. It is growing into the complex region. Sample thickness $d=100$ μm.

fected most. As the orientation of the stripe pattern rotates, the transverse instability affecting the VRL also moves around.

A note should be given about the experimental observation. At the formation of VRL TI, while one could constantly see the ripples caused by the transient stripes on the VRL, the stripe pattern in the bulk away from the VRL region still oscillates in amplitude and orientation. The stripes appear and disappear periodically. This contrast may lead one to disassociate the Transverse Instability of VRL from the transient stripe pattern. This disguise is eliminated by the following procedure in the experiment: if we grow a uniform VRL pattern and suddenly increase the magnetic field to where one expects the VRL TI, we see that the transient stripes appear everywhere. Only after some time does the distinction between the VRL TI region and the bulk become noticeable. Apparently the reason for the constant ripples of the VRL TI is the nonlinear coupling between VRL and the stripe pattern.

As a small sample thickness limits the flow coupling and suppresses the transient stripe pattern, the transverse instability of VRL in thin samples is also suppressed. For a sample of 30 μm, the transverse instability is so weak that we did not include it in the state diagram in Fig. 2. The complex pattern is also not found in thin samples, which is consistent with our previous explanation.

The VRL pattern is also affected by small sample thicknesses, although not as much as the transient stripe pattern. An obvious sign of the thickness effect is that the spatial period of the VRL in a thin sample is larger than that in a thick sample. This can be explained by a suppressed flow field in a thin sample, which means on the average a VRL lattice takes a longer time to nucleate.

The long-term stage has only one pattern, which is what we call the short-wavelength lattice (SL, Fig. 12). SL is normally nucleated from the boundary. This is the equivalent of the dynamic soliton lattice in the synchronous regime. The dominate component in this pattern is the constant phase slippage between the local director and the magnetic field. Thus a strong boundary interaction is necessary for the formation of this pattern. The SL is the most stable pattern in the asynchronous regime. It grows into the bulk and takes over either the VRL, the VRL TI, or the complex pattern. Shown in Fig. 2 there is a SL line below which the SL pattern is not observed. Because the SL is a nucleated pattern, this line suggests that the nucleation process stopped rather than that the SL cannot exist below the SL line. Since the SL is not strongly affected by flow, it has been equally observed across all sample thicknesses.

IV. CONCLUSION

The system of a nematic cell subjected to a rotating magnetic field presents a rich variety of pattern responses. In the synchronous regime, besides the dynamic soliton and its variation the spiral pattern, we found also the soliton-antisoliton pair and its variations the foam pattern and the distorted soliton lattice in thin samples. In the asynchronous regime, there are three basic pattern responses, the transient stripe pattern, the viscosity reduction lattice, and the short-wavelength lattice. The superposition of the transient stripe pattern and VRL gives the VRL transverse instability pattern, and the transient stripe pattern with extreme amplitude results in the chaotic complex pattern.

The thickness effect in the synchronous regime can be explained with a simple scaling mechanism of H_c^2 and ω_1. A smaller thickness corresponds to a larger H_c and ω_1, which enables us to study the pattern responses in the low magnetic field, low rotational speed limit. In the asynchronous regime, the thickness effect can be explained with the suppression of flow by a finite thickness. A small thickness suppresses flow and eliminates the flow-generated transient stripe pattern. Since the VRL TI and the complex pattern are variations of the transient stripe pattern, they are also suppressed in thin samples.

ACKNOWLEDGMENTS

This research is supported by the NSF through Grant No. DMR-9415656, and by the Martin Fisher School of Physics at Brandeis University.

[1] K. B. Migler and R. B. Meyer, Phys. Rev. Lett. **66**, 1485 (1991).
[2] S. Nasuno, N. Yoshimo, and S. Kai, Phys. Rev. E **51**, 1598 (1995).
[3] M. Grigutsch and R. Stannarius (unpublished).
[4] E. Pashkovsky *et al.* (unpublished).
[5] F. Brochard, L. Leger, and R. B. Meyer, J. Phys. (Paris) Colloq. **36**, C1-209 (1975).
[6] G. Srajer, S. Fraden, and R. B. Meyer, Phys. Rev. A **39**, 4828 (1989).
[7] K. B. Migler and R. B. Meyer, Phys. Rev. E **48**, 1218 (1993).
[8] C. Zheng and R. B. Meyer (unpublished).
[9] Kalman B. Migler, Ph.D. thesis, Brandeis University, 1991.
[10] K. B. Migler and R. B. Meyer, Physica D **71**, 412 (1994).
[11] C. Zheng and R. B. Meyer (unpublished).
[12] F. Lonberg, S. Fraden, A. J. Hurd, and R. B. Meyer, Phys. Rev. Lett. **52**, 1903 (1984).